Deciphering heterogeneous enzymatic surface reactions on xylan using surface plasmon resonance spectroscopy

Carbohydrate Polymers 337 (2024) 122137

Contents lists available at ScienceDirect

Carbohydrate Polymers

journal homepage: www.elsevier.com/locate/carbpol

Deciphering heterogeneous enzymatic surface reactions on xylan using surface plasmon resonance spectroscopy

Jana B. Schaubeder [a], Peter Fürk [b], Richard Amering [a], Lena Gsöls [c,d], Jonas Ravn [e], Tiina Nypelö [f,g], Stefan Spirk [a,*,1]

[a] Graz University of Technology, Institute of Bioproducts and Paper Technology (BPTI), Inffeldgasse 23, 8010 Graz, Austria
[b] Graz University of Technology, Institute for Chemistry and Technology of Materials (ICTM), Stremayrgasse 9, 8010 Graz, Austria
[c] Graz University of Technology, Institute of Molecular Biotechnology, Petersgasse 14, 8010 Graz, Austria
[d] The COMET Center, Acib GmbH, Krenngasse 37, 8010 Graz, Austria
[e] Chalmers University of Technology, Department of Life Sciences, 412 96 Gothenburg, Sweden
[f] Chalmers University of Technology, Department of Chemistry and Chemical Engineering, 412 96 Gothenburg, Sweden
[g] Aalto University, Department of Bioproducts and Biosystems, Vuorimiehentie 1, 02150 Espoo, Finland

ARTICLE INFO

Keywords:
Enzymatic degradation
Xylanases
Reaction kinetics
Multilayer thin films
Polyhydroxybutyrate
Biopolymers

ABSTRACT

Xylans' unique properties make it attractive for a variety of industries, including paper, food, and biochemical production. While for some applications the preservation of its natural structure is crucial, for others the degradation into monosaccharides is essential. For the complete breakdown, the use of several enzymes is required, due to its structural complexity. In fact, the specificity of enzymatically-catalyzed reactions is guided by the surface, limiting or regulating accessibility and serving structurally encoded input guiding the actions of the enzymes. Here, we investigate enzymes at surfaces rich in xylan using surface plasmon resonance spectroscopy. The influence of diffusion and changes in substrate morphology is studied via enzyme surface kinetics simulations, yielding reaction rates and constants. We propose kinetic models, which can be applied to the degradation of multilayer biopolymer films. The most advanced model was verified by its successful application to the degradation of a thin film of polyhydroxybutyrate treated with a polyhydroxybutyrate-depolymerase. The herein derived models can be employed to quantify the degradation kinetics of various enzymes on biopolymers in heterogeneous environments, often prevalent in industrial processes. The identification of key factors influencing reaction rates such as inhibition will contribute to the quantification of intricate dynamics in complex systems.

1. Introduction

Xylanases are enzymes that selectively cleave the β-1,4-linked backbone of xylan and are classified into different glycoside hydrolase (GH) families, depending on their amino acid sequences and structural features, with families 10 and 11 being the best known (Collins et al., 2005). The activity of the xylanases can vary depending on the species, which it is obtained from, but also on the reaction environment (pH, temperature, buffer concentration, substrate specificity, presence of inhibitors) (Chen et al., 2016; Gebruers et al., 2010). While most established methods for determining the activity of xylanases and enzymes are generally performed in solution e.g. spectrophotometric assay, DNS method, xylose equivalent release (Bailey et al., 1992; Boucherba et al., 2017), the kinetic parameters obtained are not necessarily applicable to reactions occurring in a heterogeneous environment, where enzyme reactions can be orders of magnitude slower as a result of multiple energetic and transport factors (Lee et al., 2007). Therefore, enzymatic reactions at a liquid/solid interface still need to be better understood.

To investigate heterogeneous surface reactions, different approaches are needed. One versatile technique is surface plasmon resonance spectroscopy (SPRS), which is a sensitive method capable of recording the real-time activity of enzymes on immobilized substrates. Corn and coworkers published pioneering work on kinetics simulation of SPRS data using a combination of Langmuir and Michaelis-Menten concepts (Fang et al., 2005; Lee et al., 2005; Lee et al., 2006).

Guided by these works, we aim to identify the kinetic reaction rates

* Corresponding author.
E-mail address: stefan.spirk@tugraz.at (S. Spirk).
[1] Members of NAWI Graz and the European Polysaccharide Network of Excellence (EPNOE).

https://doi.org/10.1016/j.carbpol.2024.122137
Received 1 October 2023; Received in revised form 7 March 2024; Accepted 5 April 2024
Available online 7 April 2024

for the heterogeneous enzymatic degradation of xylan. We further developed the xylan cellulose thin films from a previous study (Schaubeder et al., 2022) to quantify the xylanolytic activity of xylanases and investigate the influence of diffusion and substrate morphology on the degradation kinetics. We used the model proposed by Corn and co-workers (Lee et al., 2005) to observe if it is applicable on the degradation of a multilayered xylan film, which is a more complicated system than the 1:1 binding of enzymes to DNA microarrays. As this model does not give a good fit for most cases, we extended the model to include the use of multilayered biopolymer films instead of monolayers and include the Hill coefficient (Hill, 1910) as a factor for the positive or negative interaction between different enzymes.

To validate this extension, the model was first tested on a synthetic biopolymer thin film system, namely the degradation of polyhydroxybutyrate (PHB) with a PHB-depolymerase (PHB-DP) that is structurally less complex than xylan, that has a linear backbone, yet that is decorated with various substituents whose abundance depends on the plant source of xylan and processing method. PHB belongs to the class of polyalkanoates characterized by linear polymer chains comprised solely of 3-hydroxybutyric acid molecules, which exist in the (*R*)-enantiomeric form when naturally produced in organisms. The polymer exhibits hydrophobic and thermoplastic properties with a high degree of crystallinity, which can reach up to 80 % (dos Santos et al., 2017; McAdam et al., 2020). Considering these properties, the degradability of PHB is further influenced by a multitude of factors, including stereoregularity, crystallinity, temperature, surface accessibility and particle size (Kalia et al., 2021).

We hypothesize that the heterogeneous enzymatic surface reactions can be modeled using multilayered biopolymer thin films, validate it for PHB and demonstrate it for using xylan degradation by different xylanases to better understand the parameters affecting degradation. This will enable a more sophisticated understanding of the complex nature of heterogeneous enzymatic surface reactions and contribute to their quantification. By understanding the surface activities of enzymes and its catalytic reactions and inhibition effects, industrial processes can be adapted for better utilization or higher yield. The derived python code allows for analyzing many more heterogeneous enzymatic surface reactions and has been designed in a way that it can be used also by non-advanced programmers.

2. Derivation of the underlying reaction model

In the simplest case, heterogeneous surface reactions are defined by a general reaction scheme consisting of two steps that control the overall reaction rate. The first step is the adsorption (and desorption) of enzyme *E* from solution onto the surface bound substrate *S*, which produces a substrate-bound enzyme-substrate complex *ES* (Eq. (1)). This step can be described by Langmuir adsorption kinetics, where k_a and k_d are the Langmuir adsorption and desorption rate constants, and k_a/k_d is the Langmuir adsorption coefficient K_{Ads}. The second step is the enzymatic surface reaction of the *ES* complex to form the surface-bound product *S** via the catalytic surface reaction rate k_{cat} and the release of the enzyme back into solution (Eq. (2)) (Lee et al., 2007).

$$S + E \underset{k_d}{\overset{k_a}{\rightleftharpoons}} ES \tag{1}$$

$$ES \overset{k_{cat}}{\rightarrow} S^* + E \tag{2}$$

In general, the modeling of multistep enzymatic reactions in solution is based on the steady-state approximation. In this approximation, the enzymatic reaction is assumed to proceed in two phases: a transient initial phase in which a small amount of the *ES* complex is formed, and a steady-state phase in which the concentration of the *ES* complex remains constant over time due to the equilibrium between complex formation, dissociation, and consumption by the catalytic reaction. In addition, it is assumed that small amounts of substrate are consumed in the first pre-steady-state phase, which can be neglected. However, in heterogeneous enzymatic surface reactions where the amount of substrate bound to the surface is limited, a significant amount of substrate may be consumed before a steady-state concentration is reached in the *ES* complex. Therefore, using the steady-state approximation to model enzymatic reactions on immobilized substrates is questionable, as has been noted in the literature (Anne & Demaille, 2012; Fang et al., 2005; Gutiérrez et al., 2004; Lee et al., 2005; Lee et al., 2006).

Another complicating factor regarding liquid-solid interface reactions is that diffusion effects can occur. Therefore, a step is added to account for the mass transport of the enzyme from the solution ($E_{(x=\infty)}$) to the surface of the substrate ($E_{(x=0)}$) via the mass transport coefficient k_m (Eq. (3)) introducing a dimensionless parameter β, which describes the steady-state diffusion of the enzyme to the surface (Bourdillon et al., 1999; Lee et al., 2007).

$$E_{(x=\infty)} \overset{k_m}{\rightarrow} E_{(x=0)} \tag{3}$$

Corn and co-workers have derived the differential kinetic equations describing this three step reaction including the diffusion effects based on the relative surface coverage θ_x of the three species *S*, *ES*, and *S** (Eqs. (4), (5), and (6)) (Lee et al., 2005).

$$\theta_S + \theta_{ES} + \theta_{S^*} = 1 \tag{4}$$

$$\frac{d\theta_{ES}}{dt} = \frac{k_a\theta_S[E] - k_d\theta_{ES} - k_{cat}\theta_{ES}}{1 + \beta\theta_S} \tag{5}$$

$$\frac{d\theta_{S^*}}{dt} = k_{cat}\theta_{ES} \tag{6}$$

The relative surface coverage of species x is defined as $\theta_x = \Gamma_x/\Gamma_{tot}$, where Γ_x is the number of surface sites occupied by species x, Γ_{tot} is the total number of surface sites, and β compares the rate of adsorption and diffusion according to Eq. (7).

$$\beta = \frac{k_a\Gamma_{tot}\delta}{D} = \frac{k_a\Gamma_{tot}}{k_m} \tag{7}$$

Here, *D* is the diffusion constant of the enzyme, k_m is the steady-state mass transfer coefficient ($= D/\delta$) and δ is the steady-state diffusion layer thickness, which depends on the flow rate and the dimensions of the flow cell according to Eq. (8) (Christensen, 1997).

$$\delta = \sqrt[3]{\frac{Dh^2bl}{F}} \tag{8}$$

Here, *D* again denotes the diffusion constant of the enzyme, *h*, *b*, and *l* the height, width, and length of the flow cell, respectively, and *F* the volumetric flow. The diffusion constant of the enzyme can be estimated using Stoke's law and the Einstein-Sutherland equation (Eq. (9)) (Christensen, 1997), where M_W is the molecular weight of the enzyme, $\bar{v}$ is the specific density (normally around 7.0–7.55·10^{-4} $m^3{\cdot}kg^{-1}$ for proteins), *k* is the Boltzmann's constant (1.381·10^{-23} $J{\cdot}K^{-1}$), *T* is the absolute temperature, N_A is the Avogadro's number (6.022·$10^{23}{\cdot}mol^{-1}$), η is the viscosity (around 0.001 $kg{\cdot}s{\cdot}m^{-1}$) and f/f_0 is the friction factor of the enzyme relative to a sphere of the same size, which is usually around 1.2 for most globular proteins (Squire & Himmel, 1979).

$$D = \frac{kT}{f} = \frac{kT}{6\pi\sqrt[3]{\frac{3M_W\bar{v}}{4\pi N_A}}\eta\frac{f}{f_0}} \tag{9}$$

The kinetics simulations can then be performed using numerical integration methods with the initial conditions $\theta_S = 1$, $\theta_{ES} = \theta_S{}^* = 0$ at time $t = 0$, using Eqs. (4), (5) and (6) as proposed by Corn and co-workers, who successfully modeled data from SPRS measurements with this approach (Fang et al., 2005; Lee et al., 2005; Lee et al., 2006).

However, they had a monolayer of substrate immobilized on the SPRS sensor slides, which enabled the use of relative surface coverages. Here, we aim to expand the model to make it suitable for multilayered films, hence the denotation changes from relative surface coverage θ_x to mole fraction X_x. Additionally, the substrate S is differentiated into non-degradable substrate S_{nd} and surface substrate S_s. These modifications yield the updated modeling equations (Eqs. (10), (11), (12), and (13)). This introduction of a non-degradable substrate fraction is especially important for the xylan/xylanase system dealing with in this work, since xylan is a heterogeneous biopolymer in nature, therefore making it difficult for a single enzyme to degrade the entire macromolecule as most enzymes can only cleave a specific bond leaving behind other linkages that require different enzymes for degradation (Bhardwaj et al., 2019). The non-degradable substrate fraction is therefore the sum of all substrate fractions that cannot be degraded as a result of blocking by steric hindrance, inaccessibility, and substrate specificity, and can vary greatly depending on the biopolymer used. This model will be referred to as **Model 1** hereafter.

$$S_S + S_{nd} + E \underset{k_d}{\overset{k_a}{\rightleftharpoons}} ES + S_{nd} \overset{k_{cat}}{\rightarrow} S^* + E + S_{nd} \tag{10}$$

$$X_{S_s} + X_{S_{nd}} + X_{ES} + X_{S^*} = 1 \tag{11}$$

$$\frac{dX_{ES}}{dt} = \frac{k_a X_{S_s}[E] - k_d X_{ES} - k_{cat} X_{ES}}{1 + \beta X_{S_s}} \tag{12}$$

$$\frac{dX_{S^*}}{dt} = k_{cat} X_{ES} \tag{13}$$

Another factor that must be considered is that we are dealing with substrates that can have multiple non-identical sites per molecule for enzyme action. Therefore, an interaction parameter n was added to the reaction scheme according to Eq. (14). This enzyme-substrate interaction parameter is also known as Hill coefficient, which is widely used in pharmaceutical engineering and is a measure of the cooperativity of binding between enzyme and substrate (Hill, 1910). Consequently, the differential equation must be adjusted according to Eq. (15) and can be used directly instead of Eq. (12). The parameter n is only included in the numerator, since it is assumed to be negligible for the diffusion step in the proposed model. This model will be referred to as **Model 2** hereafter.

$$nS_S + S_{nd} + E \underset{k_d}{\overset{k_a}{\rightleftharpoons}} ES_n + S_{nd} \overset{k_{cat}}{\rightarrow} S^* + E + S_{nd} \tag{14}$$

$$\frac{dX_{ES_n}}{dt} = \frac{k_a X_{S_s}^n [E] - k_d X_{ES_n} - k_{cat} X_{ES_n}}{1 + \beta X_{S_s}} \tag{15}$$

3. Materials and methods

3.1. Materials

Xylan isolated from birchwood (DP70-1000; product code X0502) was purchased from Sigma Aldrich and used without further purification. The xylan was comprised of 89 wt% xylose with <1 wt% arabinose and <1 wt% glucose residues (90 % total carbohydrates) and contained approximately one uronic acid unit per eleven xylose units (Gabrielii, 1998; Palasingh et al., 2021). Sodium phosphate monobasic dehydrate (purum p.a., crystallized, ≥99.0 %), sodium phosphate dibasic dehydrate (BioUltra, ≥99.0 %) and bovine serum albumin (lyophilized powder ≥96 %, A2153) were purchased from Sigma Aldrich. Chloroform ($CHCl_3$, stabilized with about 0.6 % ethanol) and hydrochloric acid (HCl, 37 %) were purchased from VWR Chemicals. Dimethylsulfoxide (DMSO ≥99.5 %) and hydrogen peroxide (H_2O_2, 30 % in water) were purchased from Carl Roth. Sulfuric acid (H_2SO_4, ≥95 %) was purchased from Fisher Scientific (UK). Trimethylsilyl cellulose (TMSC, prepared by silylation of Avicel, $DS_{Si} = 2.74$, $M_w = 181{,}000$ g·mol^{-1}, $M_n = 30{,}400$ g·mol^{-1}, PDI = 6.1, determined by size exclusion chromatography in chloroform) was purchased from TITK (Rudolstadt, Germany). Endo-1,4-β-D-xylanase from *Neocallimastix patriciarum* (cat. no. E-XYLNP; $GH11_{N.p.}$) and endo-1,4-β-xylanase from *Cellvibrio japonicus* (cat. no. E-XYNACJ, $GH10_{C.j.}$) were purchased from Megazyme International (Bray, Ireland). The endo-1,4-β-xylanase from *Blastobotrys mokoenaii* $GH11_{B.m.}$ was obtained from Industrial Biotechnology division, Chalmers University of Technology, Sweden and characterized as *Bm*Xyn11A by Ravn et al. (2023). All above-mentioned chemicals were used as received. SPRS metal sensor slides (CEN102Au) with a chromium adhesion layer of approx. 5 nm on glass and a gold coating of approx. 50 nm were obtained from Cenibra (Bramsche, Germany). MilliQ water (resistivity = 18.2 MΩ·cm) from a Millipore water purification system (Millipore, USA) was used for all experiments. Poly-3-hydroxybutyrate (PHB) powder (ENMAT Y3000 PHB, $M_w = 350{,}000$ g·mol^{-1}, melting temperature 175 °C, purity 99 %) was purchased from Helian Polymers BV (Netherlands) and used without further purification. PHB-depolymerase was isolated from *Acidovorax* sp. and expressed in *E. coli Origami B* and stored in 10 mM potassium phosphate buffer pH 7.4 including 100 mM NaCl.

3.2. Thin film preparation

Xylan was dissolved in DMSO at concentrations of 20, 30, or 40 mg·ml^{-1} aided by activation with deionized water according to Schaubeder et al. (2022). PHB was directly dissolved in chloroform at a concentration of 1.25 g·l^{-1}. The solutions were directly used for spin coating. SPRS sensor slides were cleaned for 2 min with a piranha solution containing H_2O_2 (30 wt%)/H_2SO_4 (1:3 v/v) followed by rinsing with MilliQ water for several min and subsequently dried in a nitrogen stream. TMSC was dissolved in chloroform at a concentration of 0.75 wt % in an ultrasonic bath (45 W) accompanied by heating (60 °C) for approximately 6 h. The solution was then filtered with a 0.45 µm PTFE filter and the resulting solution (80 µl·cm^{-2}) was deposited on the SPRS sensor slides and subjected to spin coating (t = 60 s with a spinning speed of 4000 rpm, acceleration of 2500 rpm·s^{-1}). The TMSC films were regenerated for 14 min by exposing them to HCl vapor, generated from diluted HCl solution (10 %) (Mohan et al., 2012). The cellulose thin films produced serve as an anchoring layer to obtain homogeneous xylan films. Without further treatment, 160 µl of the corresponding xylan solution was spin coated on the cellulose film (t = 60 s, 4000 rpm, 2500 rpm·s^{-1}) according to a modified literature procedure (Rohm et al., 2014). For the PHB film, 160 µl PHB solution was directly coated onto the cleaned SPRS sensor slides.

3.3. Enzyme solutions

Endo-1,4-β-xylanase $GH11_{N.p.}$ solution with a concentration of 323 nM (5 U·ml^{-1}) was prepared in 100 mM sodium phosphate buffer, pH 6 with 0.5 mg·ml^{-1} bovine serum albumin, acting as protein stabilizing agent. Endo-1,4-β-xylanase $GH11_{B.m.}$ and $GH10_{C.j.}$ solutions with a concentration of 775 nM (5 U·ml^{-1}) were prepared in 100 mM sodium phosphate buffer, pH 5 with 0.5 mg·ml^{-1} bovine serum albumin. One unit of xylanase activity is defined as the amount of enzyme required to release one µmol of xylose reducing-sugar equivalents per minute from wheat arabinoxylan (Megazyme Ltd., Bray Business Park, Bray, Co. Wicklow, A98 YV29, Ireland). PHB-depolymerase (PHB-DP) solution with a concentration of 505 nM (0.03 U·ml^{-1}) was prepared in 200 mM sodium phosphate buffer, pH 7.4. For the SPRS experiments, a total of 200 µl enzyme solution was applied in the SPRS chamber at the corresponding flow rate and experiment time, resulting in a total of 0.006 U PHB-DP and 1 U xylanase applied per experiment.

3.4. Determination of PHB-DP activity using a photometrical assay

The specific activity of PHB-DP was determined by quantifying the product concentration formed at specific time intervals using a D-3-Hydroxybutyric Acid Assay Kit (Kientsch-Engel & Siess, 1990) obtained from Megazyme Ltd. (Bray Business Park, Bray, Co. Wicklow, A98 YV29, Ireland). Initially, 10 mg of PHB powder (ENMAT Y3000 PHB, M_w = 350,000 g·mol^{-1}, purity 99 %) was weighed in duplicates and placed in 2 ml Eppendorf tubes, followed by the addition of 1 μg of purified PHB-DP to 1 ml of 200 mM potassium phosphate buffer (PPB) pH 7.4, all conducted on ice. Subsequently, after incubating the enzyme-substrate mixture for 5 min at 4 °C with agitation at 550 rpm, the PHB powder was three times washed with cold 200 mM PPB pH 7.4 for 5 min each at 4 °C and 550 rpm. To initiate the enzymatic reaction, fresh 2 ml of 200 mM PPB pH 7.4 was added, and the samples were placed in a rotation wheel at 37 °C. At specific time intervals (15, 60, 90, and 120 min), 70 μl aliquots were extracted and frozen for subsequent analysis. The concentration of 3-hydroxybutyric acid (3HB) after different sampling time points was photometrically determined in triplicate using a Synergy plate reader in a 96-Well plate format. In the initial enzymatic reaction catalyzed by 3-hydroxybutyric acid Dehydrogenase (3-HBDH), 3HB underwent oxidation to form acetoacetate and NADH, utilizing NAD as a cofactor. In a subsequent reaction, NADH was used to reduce iodonitrotetrazolium chloride (INT) to produce an INT-formazan product, measurable at 492 nm. The quantity of INT-formazan generated during the reaction was stoichiometrically related to the amount of 3HB present in the sample. For each measurement, 10 μl of 3HB standard solution from the Megazyme assay Kit, with a concentration of 0.06 mg·ml^{-1}, was applied in triplicates. The concentration of 3HB was calculated using Lambert Beer's law, using a molar extinction coefficient of 19,900 l·mol^{-1}·cm^{-1}. The specific activity was subsequently calculated from the slope of the 3HB concentration curve observed over the 120-minute reaction period. The mean specific activity of the duplicates was 30 U·mg^{-1}, exhibiting a standard deviation of 1.2 U·mg^{-1}, equivalent to 4 %.

3.5. Multi parameter surface plasmon resonance spectroscopy – MP-SPRS

Real-time enzymatic degradation experiments were performed using an MP-SPR Navi™ 210 VASA from BioNavis Ltd. (Tampere, Finland) containing four lasers (λ = 670, 785, 850, and 980 nm) in measurement chamber A and two lasers (λ = 670, and 785 nm) in measurement chamber B. All measurements were performed at 25 °C using an angular scan range of 50 to 78° and a scan speed of 8°·s^{-1}. The SPRS experiment consists of three steps, first the coated SPRS sensor slides (glass substrate with a ~5 nm thick chromium adhesion layer and a ~50 nm thick gold layer) were equilibrated by rinsing with sodium phosphate buffer (for all xylanase experiments: 100 mM, pH 6 ($GH11_{N.p.}$) and pH 5 ($GH_{B.m.}$ and $GH10_{C.j.}$) in MilliQ and for all PHB-DP experiments: 200 mM, pH 7.4 in MilliQ) at the corresponding flow rate of 25, 50, or 100 μl·min^{-1} for about 30 min. In the second step, the enzyme solution (5 U·ml^{-1} xylanase, or 0.03 U·ml^{-1} PHB-DP in sodium phosphate buffer) was injected into the system and allowed to degrade the substrate for either 8, 4, or 2 min at a flow rate of 25, 50, or 100 μl·min^{-1}, respectively. In the third step, the substrates were again rinsed for about 30 min with sodium phosphate buffer. Triplicates were performed for each sample, resulting in a total of 6 measurements from which the mean and standard deviation were calculated. BioNavis Dataviewer software was used for data processing. De Feijter equation (Eq. (16)) was used to calculate the amount of digested xylan (mg·m^{-2}) (De Feijter et al., 1978). The change in SPRS angle ΔΘ (°) is calculated by taking the average SPRS angle from 10 min of stabilized signal before and after the experiment was performed. The term $k{\cdot}d_p$ (cm/°) can be considered constant for thin films (<100 nm) and can be calculated by calibrating the instrument by determining the decay wavelength *ld*. For the MP-SPR Navi™ 210A VASA used in this study, the $k{\cdot}d_p$ value is 1.90 × 10^{-7} cm/° for the 785 nm laser in aqueous systems. For the xylan degradation a refractive index increment (*dn/dc*) of 0.158 cm^3·g^{-1} was used as determined in an earlier study (Schaubeder et al., 2022). For degradation of PHB a *dn/dc* of 0.187 cm^3·g^{-1} was used as reported for proteins in water-based buffer systems (Robeson & Tilton, 1996). For the conversion of amount of digested substrate (determined with the De Feijter equation) to a layer thickness reduction, a density of 1.2 g·cm^3 was assumed for xylan and a density of 1.23 g·cm^3 was used for PHB (Roohi et al., 2018). The calculated degraded film thicknesses were used for kinetic simulations and are given in Table S1.

$$\Gamma = \frac{\Delta\Theta\, k\, d_p}{dn/dc} \tag{16}$$

3.6. Atomic force microscopy measurements

Atomic force microscopy (AFM) images were recorded in tapping mode using a Tosca™ 400 atomic force microscope (Anton Paar, Graz, Austria) with silicon cantilevers (AP-ARROW-NCR from NanoWorld AG, Neuchatel, Switzerland) with a nominal force constant and tip radius of 42 N·m^{-1} and < 10 μm, respectively. Image processing and surface height distributions were determined with Gwyddion v2.58 software.

3.7. Data pretreatment and kinetic simulations

The data pretreatment and fitting of the experimentally obtained data to the above-described models was carried out with Python v3.8.8 (Harris et al., 2020; Hunter, 2007; Virtanen et al., 2020; Van Rossum & Drake, 2009; The pandas development team, 2023). The dependent differential equations were solved with a 4–5-order Runge-Kutta method with given initial values. The JupyterLab file containing the data pretreatment and fitting methods is provided in the Supporting Information. For all experiments, a mean curve of a minimum of 5 measurements was used for the kinetic simulation. The data was cut to the degradation regime and normalized according to the initial layer thickness of the film to range from 1 (total film thickness) to 0 (fully degraded film). For the fitting a set of parameters is needed, such as initial film thickness [nm], degraded film thickness by the SPRS experiment [nm], enzyme concentration [M], experiment time [min], refractive index increment *dn/dc* (see Section 3.5), and the density of the corresponding thin film [g·cm^{-3}] (see Section 3.5). An overview of the parameters used for fitting is given in Table S1.

4. Results and discussion

The role of the steps involved in the degradation of heterogeneous surfaces were elucidated with resolving kinetics using the models presented in Section 2. The most sophisticated model was first validated on the degradation of PHB thin films with a PHB-depolymerase, representing a simpler system. The model was then demonstrated on the degradation of xylan at different flow rates to investigate the influence of diffusion effects (Section 4.2), on different xylan film thicknesses to draw conclusions about morphology effects (Section 4.3), and finally the efficiencies of three different xylanases were compared (Section 4.4). Fig. 1 shows a scheme of the degradation of a multilayered xylan film by a xylanase, divided into the three steps: Diffusion, adsorption/desorption, and catalytic cleavage.

4.1. Validation of Model 2 using a PHB-depolymerase on PHB

To validate the proposed model, PHB thin films with a thickness of 19 nm were treated with a PHB-DP at a concentration of 505 nM (0.03 U·ml^{-1}). We chose PHB because it is structurally less complex than xylan, so its degradation with the highly active PHB-DP potentially leads to rapid and complete degradation. The SPRS curve for the degradation (Fig. 2a) shows a strong decrease and a region with higher standard

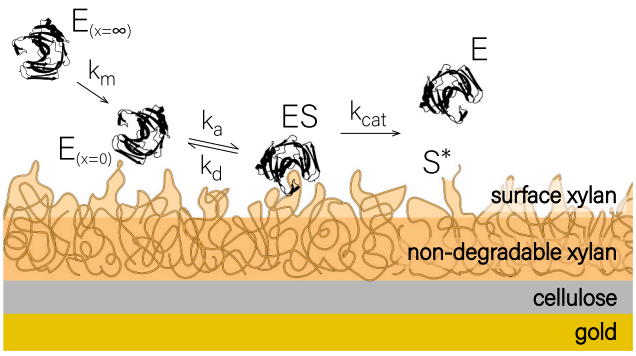

Fig. 1. Scheme of the degradation of a multilayered xylan film by a xylanase following the three steps diffusion, adsorption/desorption, and catalytic cleavage.

deviation from minute 12. The blank for this experiment was carried out by adsorbing PHB-DP on a clean SPRS sensor slide, showing strong interactions between the gold surface and the enzyme. In addition, the determined layer thickness reduction measured by SPRS (−17.8 nm) is close to the determined layer thickness measured by profilometry (19 ± 2 nm). This confirms that the complete film was degraded during this experiment and the region with the higher standard deviation at the end of the experiment corresponds to interactions between the enzyme, the gold surface, and some residue of PHB. Hence, only the degradation curve to minute 12 is considered for acquiring the fitting constants.

The quality of the fit is good for the whole measurement range (Fig. 2b, c). The evolution of the three species shows that only small amounts of X_{ES} formed (Fig. 2d), indicating that the enzyme reacts quickly after adsorption and is immediately released from the surface ($k_{cat} \gg k_a \cdot [E]^n$). The amount of surface substrate X_{SS} decreases continuously until most of the PHB is degraded, which is already after 1 min. A k_a of 105,000 $M^{-1} \cdot s^{-1}$ and a k_d of 8.1 s^{-1} were determined from the global fit using Model 2. Also, for the PHB-DP k_d is insignificantly small compared to k_a. A k_{cat} of 28.3 s^{-1} was determined. β is high with a value of 2500, indicating that diffusion effects occur. The Hill coefficient n is 0.87, indicating negative cooperativity. X_{Snd} is 25 %, which correspond to the number of PHB-DP interactions with the gold surface or rests of PHB. The total number of surface sites Γ_{tot} is 11.3 μmol·m^{-2}. Since the enzyme degraded all the PHB, the total amount of PHB degraded by the total amount of PHB-DP used during the experiment, can be calculated with the dimensions of the flow cell. This is 0.229 μg PHB (per flow cell) divided by 25 μg PHB-DP (amount of enzyme used in 2 min), which equals 9.2 ng PHB/μg PHB-DP. In contrast, the amount of PHB degraded by the PHB-DP by the photometric procedure described above (Section 3.4) is 5.124 ng PHB/μg PHB-DP (in 2 min). The proportion of amorphous and crystalline structures within PHB plays an important role in determining its degradation behavior. In the experiment involving the photometric determination of specific activities, the PHB powder was utilized without undergoing purification. In contrast, prior to SPR, the PHB powder was subjected to a purification process including drying at elevated temperatures, which may have changed the ratios of amorphous and crystalline fractions. The degradability of polyesters tends to decrease as overall crystallinity increases (Nishida & Tokiwa, 1993). Furthermore, the preferential degradation of the amorphous phase of PHB and copolymers of 3-hydroxybutyrate and 3-hydroxyvalerate has been demonstrated through ^{1}H NMR imaging (Spyros et al., 1997). Another influential factor affecting the outcome of degradation is the surface area available for interaction between the provided PHB material and PHB-DP. To achieve a maximum rate of enzymatic PHB hydrolysis, the surface must be sufficiently accessible to all enzyme molecules. The surface area of a typical PHB film used in an in vitro degradation experiment is significantly smaller than the surface area of an equivalent amount of a powdery PHB suspension (Jendrossek, 2001). Consequently, the PHB-DP concentration at which the available polymer surface becomes the limiting factor is lower for polymer films compared

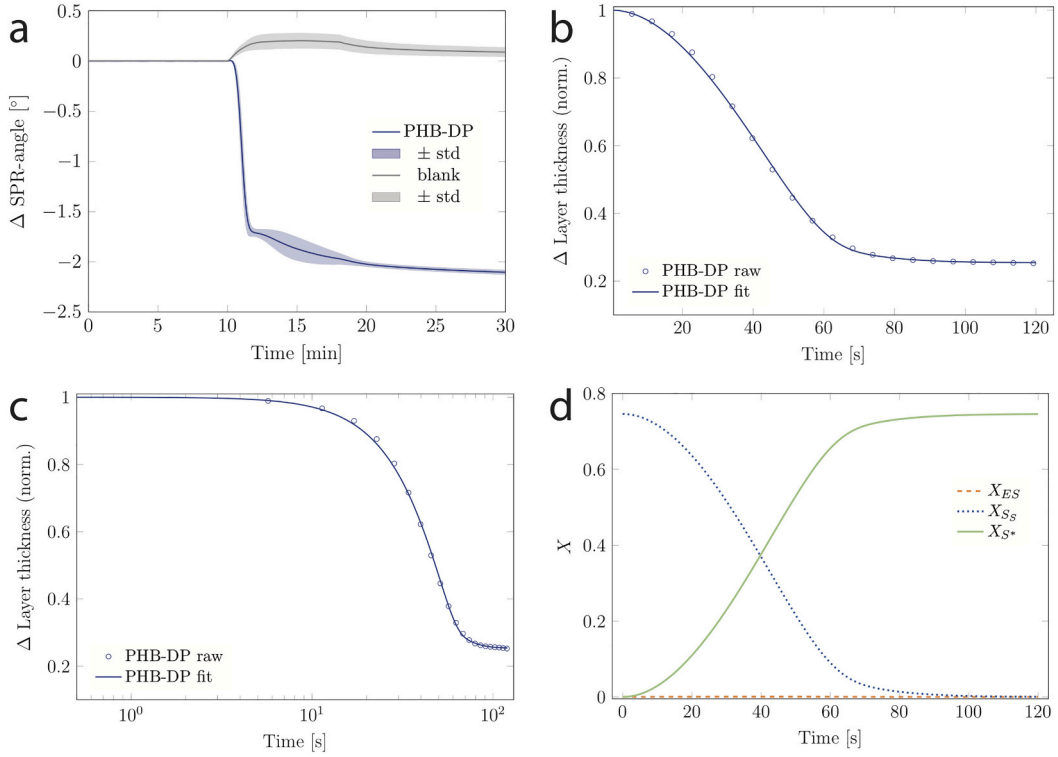

Fig. 2. (a) SPRS curve of enzymatic degradation of a PHB film with a PHB-DP and the blank by using PHB-DP on a gold substrate. Results of the global fit of the normalized SPRS data using Model 2 on a (b) linear and (c) logarithmic x-axis. (d) Evolution of the three species X_{ES}, X_{SS} and X_S* with respect to time obtained from the global fit.

to polymer suspensions (Tomasi et al., 1996). Thus, it is surprising that higher amounts of PHB were degraded by the SPRS experiment (9.2 ng PHB/µg PHB-DP) than in solution (5.12 ng PHB/µg PHB-DP), which indicates that the purification of the substrate has a significant influence on the degradation rate. Nevertheless, the values are in a comparable range, which proves the logical validity of the proposed model.

4.2. Influence of the flow rate on the kinetic parameters of xylan degradation

The differentiating shapes of the curves of the degradation of xylan by GH11$_{N.p.}$ at flow rates of 25, 50, and 100 µl·min^{-1} at the same enzyme concentration of 323 nM (5 U·ml^{-1}) confirm that it is indeed a diffusion dependent system (Fig. S1). The datasets were then analyzed by applying Model 1 (Eqs. (10), (11), (12), and (13), Fig. 3a, b) and the Model 2 (Eqs. (11), (13), (14), and (15), Fig. 3c, d) introduced in Section 2. The fitting quality is especially good at the early part of the experiment (see the logarithmic plots Fig. 3b, d). However, Model 1 cannot adequately represent the entire measurement range. Therefore, enzyme-substrate interactions are assumed to be present and Model 2 (Eqs. (11), (13), (14), and (15)) was used for global fitting.

The three degradation curves at various flow rates (Fig. 3) end at different timepoints since an equal amount of enzyme should pass over the substrate. Hence at a flow rate of 100 µl·min^{-1} the experiment lasts only 2 min where we observe a decrease in slope, indicating that the degradation is getting slower, but is probably not yet finished. Hence, less xylan was degraded in this experiment compared to the experiments at slower flow rates. The logarithmic plot (Fig. 3d) shows that the degradation reaction is delayed for the 25 µl·min^{-1} flow rate compared to the 50 and 100 µl·min^{-1} flow rates. To gain detailed insights into the degradation process, the evolution of the three different species enzyme-substrate complex X_{ES}, surface substrate X_{SS} and product X_S* is plotted over the entire experimental range (Fig. 4). For all flow rates, the number of the *ES* complex (X_{ES}) is small ($<10^{-4}$) over the experimental range; therefore, the SPRS signal can be directly used for the fitting.

The fitting constants acquired by global fitting with Model 2 are listed in Table 1. The rate constant for adsorption k_a decreases slightly with increasing flow rate (from 44,100 to 31,200 to 25,400 M^{-1}·s^{-1} for flow rates of 25, 50, and 100 µl·min^{-1}, respectively). The desorption constant k_d is about 5 orders of magnitude smaller than k_a for all flow rates indicating a strong affinity between enzyme and substrate. Hence the data are less sensitive to k_d, resulting in a higher deviation for k_d which was also the case in Fang et al. (2005), where a higher confidence interval was determined for k_d compared to k_a and k_{cat}. Therefore, we refrain here from discussing k_d for all simulations and also the related Langmuir adsorption constant K_{Ads} (=k_a/k_d) to avoid over-interpretation. The values for the catalytic constant k_{cat} vary between 23.2 s^{-1} (100 µl·min^{-1}), 34.0 (25 µl·min^{-1}), and 49.0 s^{-1} (50 µl·min^{-1}), but are in a comparable range. The diffusion coefficient β decreases from 1910 to 1100 to 860 for flow rates of 25, 50, and 100 µl·min^{-1}, respectively. According to the literature (Christensen, 1997; Karlsson et al., 1994), the diffusion coefficient should vary with flow rate and be proportional to $f^{-1/3}$, which is the case for the kinetics data obtained. Higher β values indicate faster diffusion of the enzyme to the surface of the substrate and more frequent collisions and thus faster formation of the enzyme-substrate complex. The decrease in β can be related to the decrease in k_a. At faster flow rates, diffusion of the enzyme to the surface is less frequent, so adsorption of the enzyme to form the *ES* complex is somewhat slower. The Hill coefficient n decreases with increasing flow rate from 1.19 to 0.91, to 0.59. At an n of 1, there are no cooperativity effects, i.e., at a flow rate of 25 µl·min^{-1}, there is positive cooperativity, meaning that if an enzyme is already bound to a substrate, it is more

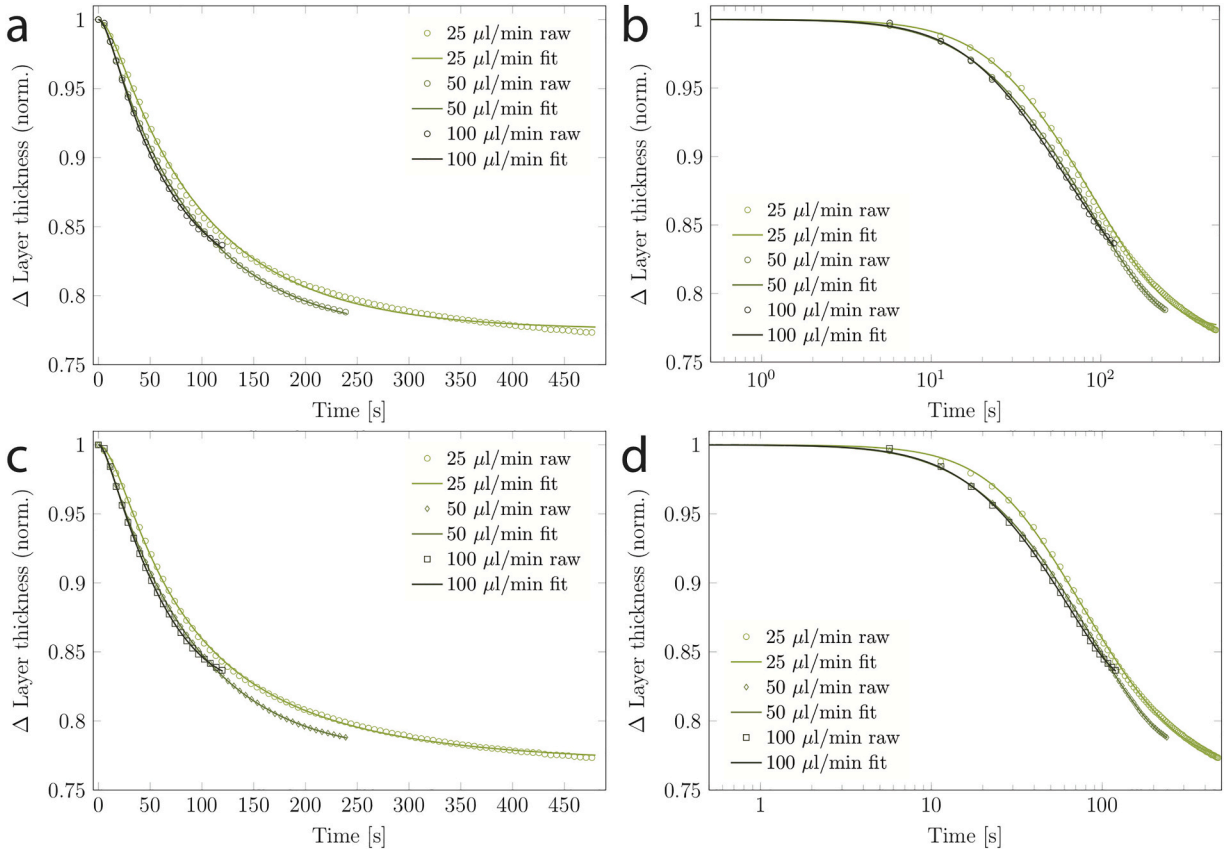

Fig. 3. Xylan thin films treated with a GH11$_{N.p.}$ xylanase at three different flow rates. Global fitting of the normalized SPRS data using (a, b) Model 1 or (c, d) Model 2, plotted on a (a, c) linear and (b, d) logarithmic x-axis, respectively.

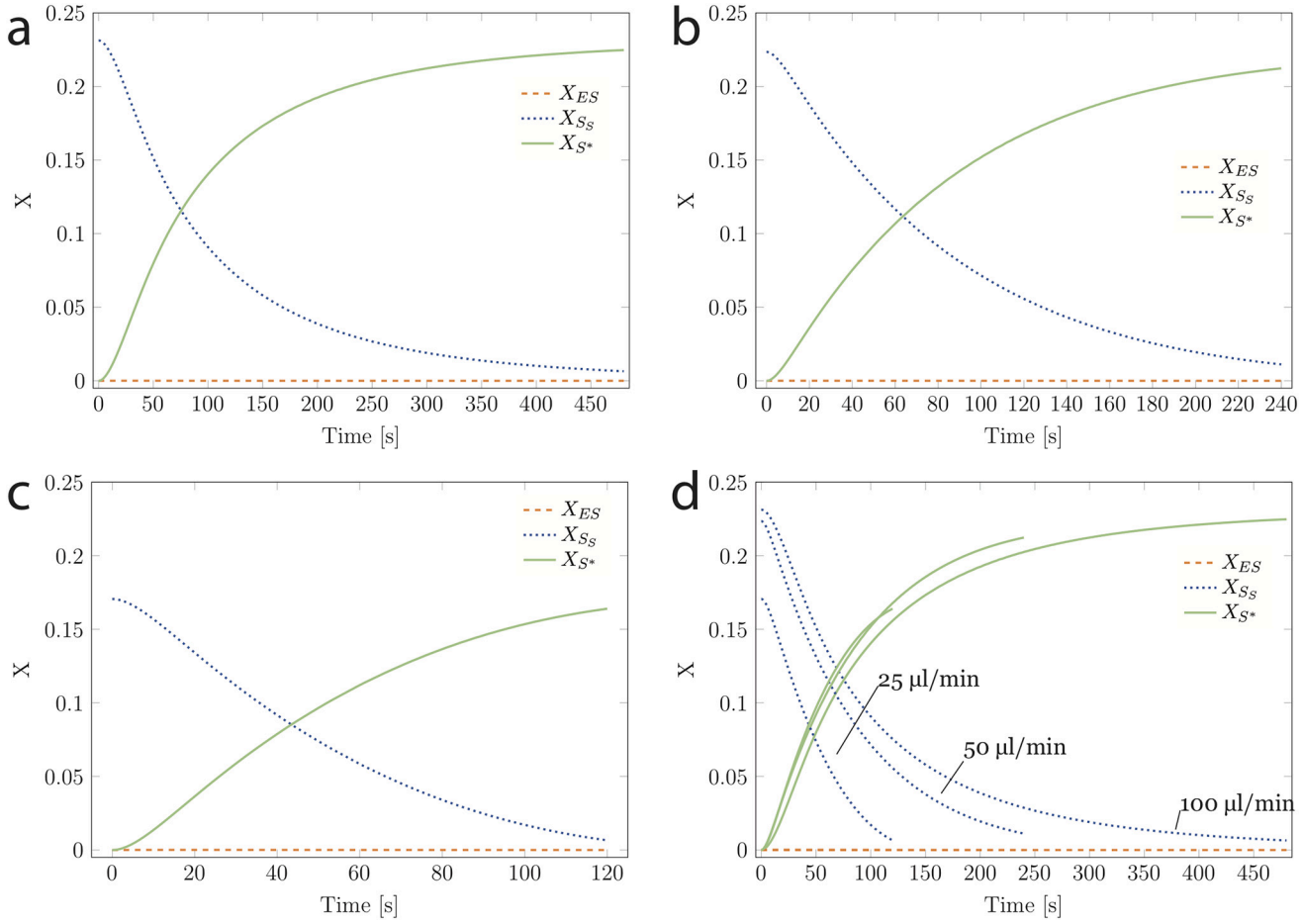

Fig. 4. Evolution of the three species X_{ES}, X_{SS} and X_S* with respect to time for xylan degradation by a GH11$_{N.p.}$ xylanase calculated with the determined fitting constants at different flow rates of (a) 25 µl·min^{-1}, (b) 50 µl·min^{-1}, (c) 100 µl·min^{-1}, and (d) all curves plotted together using Model 2.

Table 1
Fitting constants k_a, k_d, k_{cat}, β, n, non-degradable substrate fraction X_{Snd}, and resulting total number of surface sites Γ_{tot} of the 20 nm thick xylan film degraded with a GH11$_{N.p.}$ xylanase at different flow rates determined from the global fitting using Model 2.

Flow rate [µl·min^{-1}]	k_a [M^{-1}·s^{-1}]	k_d [s^{-1}]	k_{cat} [s^{-1}]	β [–]	n [–]	X_{Snd} [%]	Γ_{tot} [µmol·m^{-2}]
25	44,100	0.4	34.0	1910	1.19	77	23.8
50	31,200	1.9	49.0	1100	0.91	78	24.4
100	25,400	2.2	23.2	860	0.59	83	29.5

likely that another enzyme will bind to the same substrate. When the flow rate increases to 50 µl·min^{-1}, the Hill coefficient decreases to 0.91, which could mean that cooperativity has a smaller influence on degradation (n is close to 1). When the flow rate is further increased to 100 µl·min^{-1}, n decreases to 0.59, indicating negative cooperativity, which also decreases the overall degradation rate. The non-degradable fraction of the thin film X_{Snd} is similar at flow rates of 25 and 50 µl·min^{-1} (77 and 78 % respectively), but increases to 83 % for a flow rate of 100 µl·min^{-1}. This can be explained by the shorter experimental time of 2 min, during which less substrate could be degraded, which is visible in the SPRS curves (Fig. S1). To check the obtained kinetics data for their logical validity, the total number of surface sites Γ_{tot} was calculated, which corresponds to the sites where it is possible for the enzyme to cleave the xylan backbone. First, the height of the steady-state diffusion layer (δ) is needed for the different flow rates, which can be calculated according to Eq. (8) using the dimensions of the flow cell (length: 7.01 mm, width: 1.4 mm, height: 0.15 mm, according to the manufacturer) and the diffusion coefficient D for the GH11$_{N.p.}$ of 9.33·10^{-12} m^2·s^{-1} (according to Eq. (9) with a molecular weight of 25,800 g·mol^{-1}, at a temperature of 25 °C, and with the specified values from Section 2). With these values, the steady-state diffusion layers δ would be 17.0 µm, 13.5 µm, and 10.7 µm for flow rates of 25, 50, and 100 µl·min^{-1}, respectively. Fang et al. (2005) estimated a diffusion layer of 28 µm for the 200 µm deep SPR flow cell at a flow rate of 30 µl·min^{-1}, which is in a comparable range. We can then use δ to calculate the mass transfer coefficient k_m (=D/δ). We obtain k_m values of 0.55, 0.69, and 0.87 µm·s^{-1}, for the investigated flow rates of 25, 50, and 100 µl·min^{-1}, respectively, which corresponds to the speed of the mass diffusion process. Since β and k_a are linked to the total number of surface sites Γ_{tot} via Eq. (7), we can calculate Γ_{tot} with the fitted values of β and k_a and the calculated value for k_m. The determined Γ_{tot} values are reported in Table 1, where similar values are obtained for the different flow rates (23.8, 24.4, and 29.5 µmol·m^{-2} for a flow rate of 25, 50, and 100 µl·min^{-1}, respectively), supporting the logical validity of the acquired kinetics data, since the same xylan films with a thickness of 20 nm are used for all diffusion experiments and the same enzyme is used, thus their Γ_{tot} should be

similar. The kinetics data obtained using the simplest model proposed in Section 2 are shown in Table S2, where comparable values were obtained for flow rates of 25 and 50 µl·min^{-1}, but for a flow rate of 100 µl·min^{-1} the value for k_a is three times higher, so Γ_{tot} is much smaller, which does not make logical sense. This is another indicator that the data obtained with Model 2 better represents the actual kinetic processes.

Summarizing the results of the global fit for the different flow rates, the overall kinetics are indeed affected by diffusion effects. Comparable k_{cat} values between 23 and 49 s^{-1} were obtained, but the Hill coefficient decreases with increasing flow rate, suggesting that higher flow rates slow down the overall reaction kinetics.

4.3. Influence of the xylan layer thickness on the kinetic parameters

Xylan thin films with different surface morphologies (films of different thicknesses of 12, 20, and 40 nm) were treated with the GH11$_{N.p.}$ xylanase at a concentration of 323 nM (5 U·ml^{-1}) at a constant flow rate of 25 µl·min^{-1} to draw conclusions on the influence of substrate morphology. The SPRS data (Fig. 5a) shows that larger amounts of xylan are degraded with increasing film thickness. An overall satisfactory fitting quality is obtained for the different film thicknesses using Model 2 (Fig. 5b, c). However, at the beginning of the experiment (Fig. 5c), the fit for the thickest layer of 40 nm cannot adequately represent the curve, indicating that activities are probably taking place that are not accounted for in the model. The difference between these films is not only a matter of thickness, but also of surface morphology. It should be noted that the xylan used did not form smooth films. On the contrary; the use of different xylan concentration for spin coating resulted in thin films with different height profiles. The height distribution of the cellulose base layer is much smaller than that of the xylan layers, indicating that the bottom cellulose film is smooth (Fig. S2). It is known that the cellulose films prepared from TMSC exhibit smooth surfaces (Kontturi et al., 2006; Schaubeder et al., 2022). The higher the xylan concentration, the broader the resulting height distribution (Fig. S2), leading to larger variation in surface morphology, which in turn could alter the accessibility by the enzyme or affect diffusion processes at the liquid/solid interface.

The fitted data (Fig. 5b, c) indicates that the 12 nm and 40 nm films exhibit similar final relative thickness reductions, both reaching 80 %. The 20 nm film showed the largest relative degradation (to 77 %). The logarithmic plots (Fig. 5c) show that degradation starts fastest at the 12 nm thick film and slowest at the 40 nm film. However, in the middle region of the experiment (seconds 25 to 200), the 12 nm film shows a linear decrease in the logarithmic plot, while the 20 and 40 nm thick films show a steeper decrease, indicating that the reaction slows down for the 12 nm film in this region. At the end of the experiment, the 12 nm film shows the largest negative slope in the logarithmic plot, while the degradation slows down for the 20 and 40 nm thick films.

The evolution of the three species X_{ES}, X_{SS} and X_S* plotted with respect to time (Fig. 6) shows that the amount of the *ES* complex is small ($<10^{-4}$) throughout the experimental period (as in Section 4.2). However, zooming into the evolution of X_{ES} (Fig. S3), the number of enzyme-substrate complex increases with increasing layer thickness to a maximum and then decreases continuously until the end of the experiment. This initial increase in X_{ES} can be related to the slower onset of degradation with increasing film thickness, which is also evident from X_{SS} in Fig. 6. When the total number of surface sites (Γ_{tot}) is higher, more *ES* complexes can form simultaneously, resulting in a delayed onset of the curve decay. Another difference is that the surface-bound substrate X_{SS} does not converge to zero at the end of the experiment for the 12 nm thick film (Fig. 6a), indicating that the surface xylan was still present but degradation was hindered. This would further suggest that inhibitory processes are likely to occur at this film thickness.

The fitting constants for the different film thicknesses acquired by global fitting with Model 2 are listed in Table 2. The adsorption constant

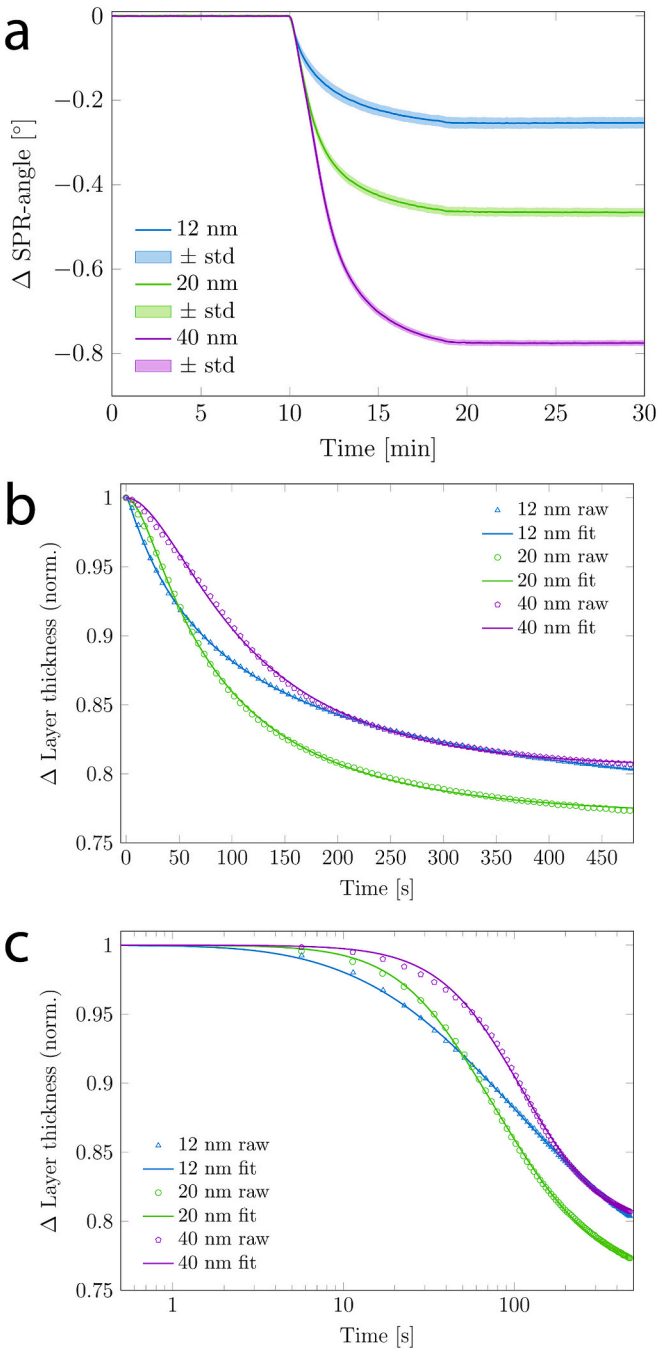

Fig. 5. (a) SPRS curves of enzymatic degradation of xylan films of different thicknesses with a GH11$_{N.p.}$ xylanase. Results of the global fit of the normalized SPRS data using Model 2 on a (b) linear and (c) logarithmic x-axis.

k_a decreases significantly with increasing xylan film thickness (from 283,000 to 44,100 to 25,000 M^{-1}·s^{-1} for thicknesses of 12, 20, and 40 nm, respectively). This indicates a higher affinity between enzyme and substrate for the thinnest film, so that the frequency of encounter between enzyme and substrate decreases with increasing film thickness. This could be a consequence of a different aggregation of xylan during spin coating from different concentrations, making the xylan coated with the lowest concentration better aligned for cleavage by the enzyme. The reaction constant k_{cat} for the cleavage of xylan also decreases significantly from 116 to 34.0 to 13.8 s^{-1} for thicknesses of 12, 20, and 40 nm, respectively. This would be consistent with the hypothesis of better accessibility of the xylan film coated with the lowest concentration. Comparison of the obtained fitting constant k_{cat} with values from

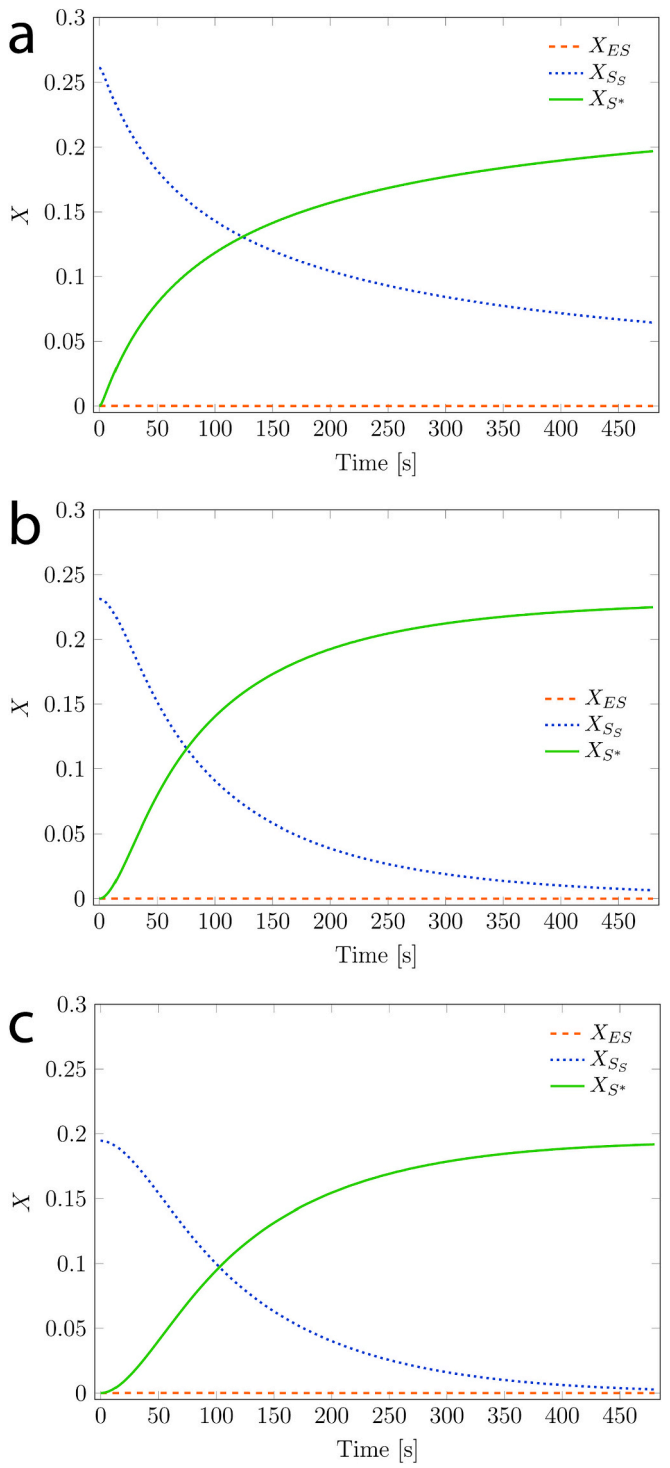

Fig. 6. Evolution of three species X_{ES}, X_{SS} and X_S* with respect to time obtained from global fitting of xylan films with different thicknesses of (a) 12 nm, (b) 20 nm, and (c) 40 nm treated with a GH11$_{N.p.}$ xylanase calculated with the determined fitting constants using Model 2.

the literature is not straightforward because the catalytic activity of different xylanases can vary widely. However, to give an idea of the magnitude, values of 55 to 106 s^{-1} (Huang et al., 2019), 480 to 3460 s^{-1} (Zhang et al., 2021), and 433 to 905 s^{-1} (Song et al., 2012) were reported for the degradation of beechwood xylan in solution. This indicates that the reactions at the solid/liquid interface are slower than in solution, as usual, probably because of limited accessibility and diffusion. The diffusion coefficient β increases from 998 to 1910 to 2120 with increasing film thickness, which means that diffusion is much faster for the 20 and 40 nm thick films compared to the 12 nm film. This change in β can be related to the different surface morphologies. As discussed above, the height distribution is broadening with increasing layer thickness, which could affect the diffusion of the enzyme to the surface of the substrate. The Hill coefficient decreases for the 12, 20, and 40 nm thick xylan films from 2.47 to 1.19 to 0.94, respectively. This would mean that the 12 and 20 nm films exhibit a positive cooperativity, with a switch to a negative cooperativity for the 40 nm film. This again suggests that the xylan coated from the solution with the lowest concentration has better accessibility or different aggregation, allowing more enzymes to interact with the same xylan macromolecule. In addition, the higher the xylan concentration used for spin coating, the poorer the affinity and accessibility of the enzyme to the substrate. The non-degradable fraction X_{Snd} is increasing slightly with increasing film thickness from 74 to 77 to 81 %, indicating that the higher the xylan concentration used for spin coating, the less of the film can be degraded. The Γ_{tot} values were determined as described in Section 4.1 and are increasing with increasing film thickness from 1.93 to 23.8 to 46.4 μmol·m^{-2}. This supports the logical validity of the determined kinetics data, since the total number of surface sites should increase with increasing xylan film thickness as a result of the broader height distributions.

Summarizing the results of the global fit of the different film thicknesses, it can be observed that the reaction kinetics are fastest for the 12 nm (thinnest) film (highest k_{cat}, k_a, and $n > 1$), with an instantaneous degradation onset and only small amounts of X_{ES} formed. Since $k_{cat} \gg k_a \cdot [E]^n$, the enzyme reacts quickly after adsorption and is immediately released from the surface. In addition, the reaction appears to be limited in the middle (seconds 25 to 200) region of the experiment, which can be attributed to the smaller surface area and lower amounts of total number of surface sites. In contrast, the relative enzymatic degradation slows down with increasing film thickness and thus with increasing concentration of the xylan solution used for spin coating, as poorer accessibility of the xylan for the enzyme occurs caused by aggregation effects. The Hill coefficient also decreases with increasing film thickness, with the value for the 40 nm (thickest) film being lower than 1, indicating that the enzymes negatively affect each other and inhibitory activities likely occur during degradation. In addition, the total number of surface sites (Γ_{tot}, Table 2) increases with film thickness, so that more X_{ES} is formed at the beginning of the reaction (Fig. S3) and the overall signal appears delayed.

4.4. Demonstration of Model 2 for xylan degradation using different xylanases

The 20 nm thick xylan films were also treated with another GH11 xylanase obtained from *Blastobotrys mokoenaii* (GH11$_{B.m.}$) and a GH10 xylanase from *Cellvibrio japonicas* (GH10$_{C.j.}$) both at a concentration of 775 nM (5 U·ml^{-1}) at a constant flow rate of 25 μl·min^{-1}. The SPRS data (Fig. 7a) shows that lower amounts of xylan were degraded with these xylanases than with the GH11$_{N.p.}$ xylanase used above. The normalized raw data and the corresponding global fits obtained using Model 2 show an overall good fitting quality for the different xylanases (Fig. 7b, c). The fitted data exhibit different final relative thickness reductions to 86 % (GH10$_{C.j.}$), 83 % (GH11$_{B.m.}$) and 77 % (GH11$_{N.p.}$). Moreover, the fastest reaction onset was determined for the GH11$_{B.m.}$ xylanase, while the GH11$_{N.p.}$ and GH10$_{C.j.}$ xylanases show an almost identical degradation onset (see the logarithmic plots Fig. 7c). However, after about 30 s the curves of GH10$_{C.j.}$ and GH11$_{B.m.}$ show a linear decrease in the logarithmic plot (Fig. 7c), while the GH11$_{N.p.}$ shows a steeper decrease, indicating inhibition reactions taking place that slow down the overall degradation rate.

The evolution of the three species X_{ES}, X_{SS} and X_S* of the GH11$_{B.m.}$ and GH10$_{C.j.}$ xylanases is plotted with respect to time (Fig. 7d). As in Sections 4.2 and 4.3, the amount of the *ES* complex is small ($<10^{-4}$) throughout the experimental period. However, zooming into the

Table 2
Calculated kinetic parameters k_a, k_d, k_{cat}, β, n, non-degradable substrate fraction X_{Snd}, and resulting total number of surface sites Γ_{tot} at different xylan film thicknesses treated with a GH11$_{N.p}$ xylanase determined from the global fitting using Model 2.

Film thickness [nm]	k_a [$M^{-1}\cdot s^{-1}$]	k_d [s^{-1}]	k_{cat} [s^{-1}]	β [−]	n [−]	X_{Snd} [%]	Γ_{tot} [$\mu mol\cdot m^{-2}$]
12	283,000	35.0	116	998	2.47	74	1.93
20	44,100	0.4	34.0	1910	1.19	77	23.8
40	25,000	2.1	13.8	2120	0.94	81	46.4

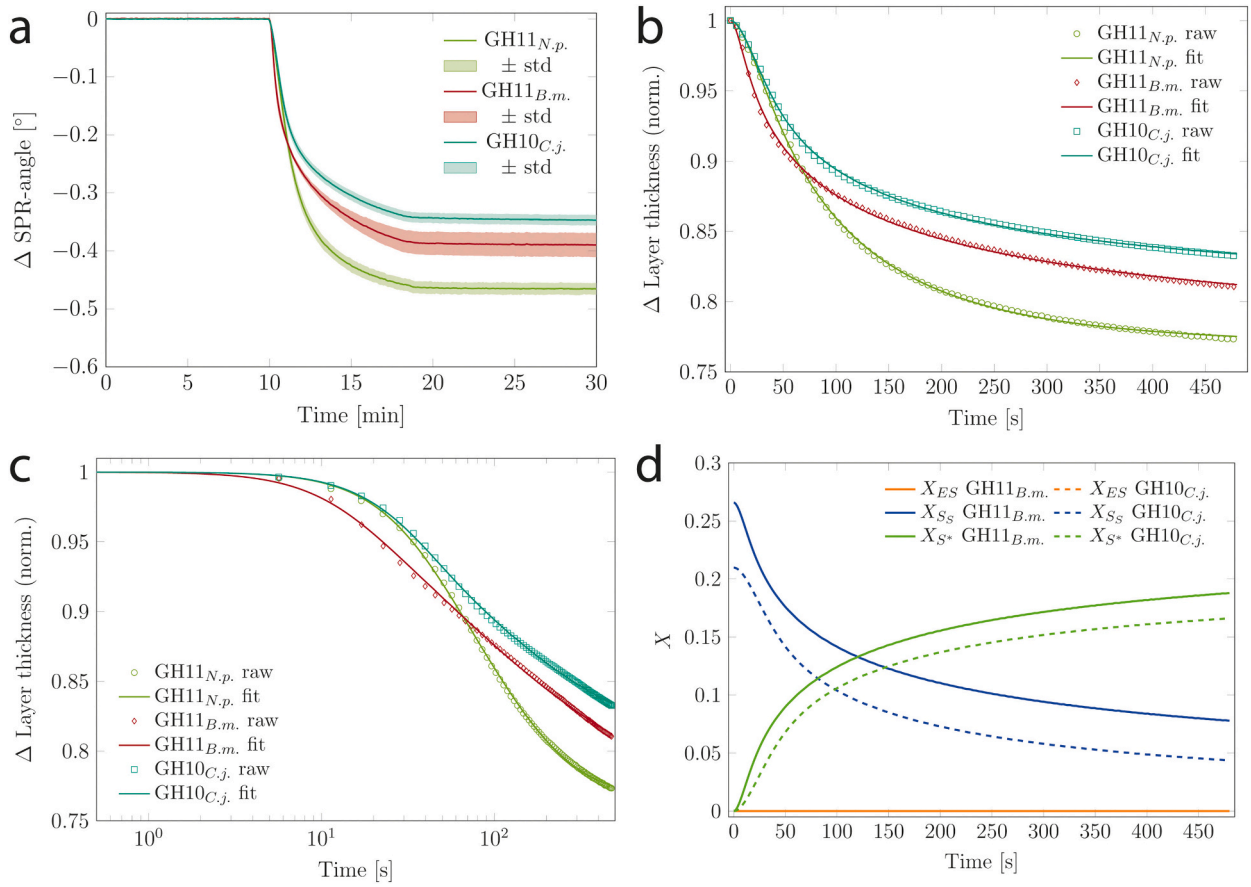

Fig. 7. (a) SPR curves of enzymatic degradation of 20 nm thick xylan films with different xylanases. Global fits of the normalized SPRS data using Model 2 on a (b) linear and (c) logarithmic x-axis. (d) Evolution of the three species X_{ES}, X_{SS} and X_S* with respect to time obtained from global fitting of xylan films treated with a GH11$_{B.m.}$ and a GH10$_{C.j.}$ xylanase calculated with the determined fitting constants using Model 2.

evolution of X_{ES} (Fig. S4), the amount of enzyme-substrate complex is similar for GH11$_{N.p.}$ and GH10$_{C.j.}$, but much lower for GH11$_{B.m.}$, suggesting that for the GH11$_{B.m.}$ xylanase a lower total amount of surface sites (Γ_{tot}) is available, resulting in less *ES* complex formation and a faster degradation onset. Moreover, the surface-bound substrate X_{SS} does not converge to zero at the end of the experiment for both, the GH11$_{B.m.}$ and the GH10$_{C.j.}$ xylanases, indicating that surface xylan was still present but degradation was hindered.

The fitting constants for the different xylanases acquired by global fitting with Model 2 (Table S3) show significant differences. The adsorption constant k_a of 339,000 $M^{-1}\cdot s^{-1}$ is highest for the GH11$_{B.m.}$ xylanase indicating a stronger affinity between enzyme and substrate for the GH11$_{B.m.}$ followed by GH10$_{C.j.}$ with a k_a of 137,000 $M^{-1}\cdot s^{-1}$ and the lowest k_a for GH11$_{N.p.}$ (44,100 $M^{-1}\cdot s^{-1}$). A similar reaction constant k_{cat} for the cleavage of xylan is determined for the GH10$_{C.j.}$ and the GH11$_{N.p.}$ xylanase (33.4 s^{-1} and 34.0 s^{-1}, respectively), while k_{cat} was twice as high for the GH11$_{B.m.}$ (96.1 s^{-1}). GH11$_{B.m.}$ has been found to have a significantly higher specific activity for beechwood xylan compared to another closely related GH11 xylanase (Ravn et al., 2023). The diffusion coefficient β exhibits similar values for the different xylanases and lies between 1910, 1930 and 2150 for GH11$_{N.p.}$, GH11$_{B.m.}$, and GH10$_{C.j.}$, respectively. As xylan films of the same thickness were used for the experiments, similar β values were to be expected. The slightly higher value for the GH10$_{C.j.}$ could be related to the slightly higher molecular weight of the xylanase (39 kDa) compared to the other xylanases with molecular weights of 21.6 kDa and 25.8 kDa for the GH11$_{B.m.}$ and GH11$_{N.p.}$, respectively. Higher Hill coefficients of 2.41 and 3.24 are determined for the GH10$_{C.j.}$ and GH11$_{B.m.}$, respectively, compared to the Hill coefficient of 1.19 for GH11$_{N.p.}$. However, all xylanases exhibit a positive cooperativity, which is most pronounced for the GH11$_{B.m.}$. This underlines the faster degradation onset for this xylanase. The non-degradable fraction X_{Snd} is similar for all xylanases at 73 %, 77 %, and 79 % for the GH11$_{B.m.}$, GH11$_{N.p.}$, and GH10$_{C.j.}$, respectively. The Γ_{tot} values are determined as described in Section 4.2 with diffusion coefficients D of $9.91\cdot10^{-12}$ $m^2\cdot s^{-1}$ for GH11$_{B.m.}$ and $8.13\cdot10^{-12}$ $m^2\cdot s^{-1}$ for GH10$_{C.j.}$ (according to Eq. (9) with a molecular weight of 21,550 $g\cdot mol^{-1}$, and 39,000 $g\cdot mol^{-1}$ for GH11$_{B.m.}$ and GH10$_{C.j.}$, respectively, at a temperature of 25 °C). This results in Γ_{tot} values of 3.24 and 7.84

μmol·m^{-2} for the GH11$_{B.m.}$ and GH10$_{C.j.}$ xylanase, respectively, which are much lower than the total number of surface sites for the GH11$_{N.p.}$ xylanase of 23.8 μmol·m^{-2}, suggesting inhibitory effects occur that reduce the available surface sites for the GH11$_{B.m.}$ and GH10$_{C.j.}$ compared to the GH11$_{N.p.}$.

In summary, significant differences in degradation efficiency were determined for the different xylanases, with the fastest kinetics for GH11$_{B.m.}$ (highest k_{cat}, k_a, and n). These xylanases show a high positive cooperativity, react quickly after adsorption and are immediately released from the surface ($k_{cat} \gg k_a \cdot [E]^n$). However, the reaction appears to be limited after about 30 s, which is not the case with GH11$_{N.p.}$ xylanase. The GH10$_{C.j.}$ xylanase shows a similar onset of degradation as GH11$_{N.p.}$, but exhibits a higher k_a and n value. However, the number of surface sites is lower, which slows down the overall degradation rate.

5. Conclusion

A model for acquiring the kinetics for the degradation of multilayered biopolymer thin films by a global fit of the SPRS data was developed and validated on the degradation of PHB with a PHB-DP. The determined kinetics of xylan degradation revealed that surface morphology of the substrate modulates degradation kinetics as it affects diffusion and accessibility. Exemplary, the reaction constant k_{cat} for the degradation of birchwood xylan by a GH11$_{N.p.}$ xylanase varied from 14 to 116 s^{-1} depending on the substrate properties. It is immediately apparent here how difficult it is to compare kinetics data from different literature sources. As a consequence, we advise to only compare kinetic values obtained with an identical measurement setup, as here, where the comparison of the degradation efficiency of three different xylanases on the same substrate showed significant differences. To make this task more appealing to a wider research group, we provide the final python code used for data processing and fitting of the kinetic parameters. The code can be easily operated and should motivate to make the first step into enzyme kinetics. However, we want to emphasize that a model with an increasing number of fitting parameters will be prone to overfitting, which amplifies the importance of evaluating the physical limitations of each coefficient and limiting the parameters accordingly.

This work will help to predict the behavior of an enzyme under different conditions by identifying the key factors that influence the reaction rate, such as diffusion and substrate concentration, but could also be extended to pH and temperature. Once identified, this powerful tool will enable a more nuanced understanding of the complex nature of the underlying mechanisms of heterogeneous enzymatic surface reactions and open up new possibilities for the optimization of industrial processes.

CRediT authorship contribution statement

Jana B. Schaubeder: Conceptualization, Formal analysis, Investigation, Methodology, Software, Validation, Writing – original draft, Writing – review & editing. **Peter Fürk:** Writing – review & editing, Software, Formal analysis. **Richard Amering:** Software, Formal analysis, Data curation. **Lena Gsöls:** Writing – review & editing, Writing – original draft, Validation, Investigation. **Jonas Ravn:** Writing – review & editing, Writing – original draft, Conceptualization. **Tiina Nypelö:** Writing – review & editing, Formal analysis. **Stefan Spirk:** Writing – review & editing, Writing – original draft, Supervision, Funding acquisition, Formal analysis.

Declaration of competing interest

The authors declare that they have no known competing financial interests or personal relationships that could have appeared to influence the work reported in this paper.

Data availability

Data will be made available on request.

Acknowledgement

The authors acknowledge Helmut Schwab for his help with the PHB studies. The authors would like to acknowledge use of the Somapp Lab, a core facility supported by the Austrian Federal Ministry of Education, Science and Research, the Graz University of Technology, the University of Graz and Anton Paar GmbH.

Funding

This work has received funding from the European Union's Horizon 2020 – Research and Innovation Framework Programme under grant agreement No 964430. Next Generation Bioproduction is funded by BMK, BMDW, SFG, Standortagentur Tirol, Government of Lower Austria und Vienna Business Agency in the framework of COMET - Competence Centers for Excellent Technologies. The COMET-Funding Program is managed by the Austrian Research Promotion Agency FFG.

Appendix A. Supplementary data

Supplementary data to this article can be found online at https://doi.org/10.1016/j.carbpol.2024.122137.

References

Anne, A., & Demaille, C. (2012). Kinetics of enzyme action on surface-attached substrates: A practical guide to progress curve analysis in any kinetic situation. *Langmuir, 28*(41), 14665–14671.

Bailey, M. J., Biely, P., & Poutanen, K. (1992). Interlaboratory testing of methods for assay of xylanase activity. *Journal of Biotechnology, 23*(3), 257–270.

Bhardwaj, N., Kumar, B., & Verma, P. (2019). A detailed overview of xylanases: An emerging biomolecule for current and future prospective. *Bioresources and Bioprocessing, 6*(1), 40.

Boucherba, N., Gagaoua, M., Bouanane-Darenfed, A., Bouiche, C., Bouacem, K., Kerbous, M. Y., … Benallaoua, S. (2017). Biochemical properties of a new thermo- and solvent-stable xylanase recovered using three phase partitioning from the extract of Bacillus oceanisediminis strain SJ3. *Bioresources and Bioprocessing, 4*(1), 29.

Bourdillon, C., Demaille, C., Moiroux, J., & Savéant, J.-M. (1999). Activation and diffusion in the kinetics of adsorption and molecular recognition on surfaces. Enzyme-amplified electrochemical approach to biorecognition dynamics illustrated by the binding of antibodies to immobilized antigens. *Journal of the American Chemical Society, 121*(11), 2401–2408.

Chen, Q., Li, M., & Wang, X. (2016). Enzymology properties of two different xylanases and their impacts on growth performance and intestinal microflora of weaned piglets. *Animal Nutrition, 2*(1), 18–23.

Christensen, L. L. H. (1997). Theoretical analysis of protein concentration determination using biosensor technology under conditions of partial mass transport limitation. *Analytical Biochemistry, 249*(2), 153–164.

Collins, T., Gerday, C., & Feller, G. (2005). Xylanases, xylanase families and extremophilic xylanases. *FEMS Microbiology Reviews, 29*(1), 3–23.

De Feijter, J. A., Benjamins, J., & Veer, F. A. (1978). Ellipsometry as a tool to study the adsorption behavior of synthetic and biopolymers at the air–water interface. *Biopolymers, 17*(7), 1759–1772.

dos Santos, A. J., Oliveira Dalla Valentina, L. V., Hidalgo Schulz, A. A., & Tomaz Duarte, M. A. (2017). From obtaining to degradation of PHB: Material properties. Part I. *Ingeniería y Ciencia, 13*, 269–298.

Fang, S., Lee, H. J., Wark, A. W., Kim, H. M., & Corn, R. M. (2005). Determination of ribonuclease H surface enzyme kinetics by surface plasmon resonance imaging and surface plasmon fluorescence spectroscopy. *Analytical Chemistry, 77*(20), 6528–6534.

Gabrielii, I. (1998). *Hydrogels based on hardwood hemicelluloses. Department of Polymer Technology (Vol. Master)*. Göteborg: Chalmers University of Technology.

Gebruers, K., Dornez, E., Bedő, Z., Rakszegi, M., Courtin, C. M., & Delcour, J. A. (2010). Variability in xylanase and xylanase inhibition activities in different cereals in the HEALTHGRAIN diversity screen and contribution of environment and genotype to this variability in common wheat. *Journal of Agricultural and Food Chemistry, 58*(17), 9362–9371.

Gutiérrez, O. A., Chavez, M., & Lissi, E. (2004). A theoretical approach to some analytical properties of heterogeneous enzymatic assays. *Analytical Chemistry, 76*(9), 2664–2668.

Harris, C. R., Millman, K. J., van der Walt, et al. (2020). Array programming with Numpy. *Nature, 585*, 357–362.

Hill, A. V. (1910). The possible effects of the aggregation of the molecules of hemoglobin on its dissociation curves. *The Journal of Physiology, 40*, iv–vii.
Huang, Y., Zheng, X., Pilgaard, B., Holck, J., Muschiol, J., Li, S., & Lange, L. (2019). Identification and characterization of GH11 xylanase and GH43 xylosidase from the chytridiomycetous fungus, Rhizophlyctis rosea. *Applied Microbiology and Biotechnology, 103*(2), 777–791.
Hunter, J. D. (2007). Matplotlib: A "D Graphics Environment. *Computing in Science & Engineering, 9*(3), 90–95.
Jendrossek, D. (2001). In W. Babel, & A. Steinbüchel (Eds.), *Biopolyesters. Advances in Biochemical Engineering/Biotechnology, 71*. Berlin, Heidelberg: Springer. https://doi.org/10.1007/3-540-40021-4_10.
Kalia, V. C., Singh Patel, S. K., Shanmugam, R., & Lee, J.-K. (2021). Polyhydroxyalkanoates: Trends and advances toward biotechnological applications. *Bioresource Technology, 326*, Article 124737.
Karlsson, R., Roos, H., Fägerstam, L., & Persson, B. (1994). Kinetic and concentration analysis using BIA technology. *Methods, 6*(2), 99–110.
Kientsch-Engel, R. I., & Siess, E. A. (1990). D-(−)-3-hydroxybutyrate and acetoacetate. In H. U. Bergmeyer (Ed.), *Methods of enzymatic analysis* (pp. 60–69). Cambridge, UK: VCH Publishers (UK), Ltd.
Kontturi, E., Tammelin, T., & Österberg, M. (2006). Cellulose—Model films and the fundamental approach. *Chemical Society Reviews, 35*(12), 1287–1304.
Lee, H. J., Wark, A. W., & Corn, R. M. (2006). Creating advanced multifunctional biosensors with surface enzymatic transformations. *Langmuir, 22*(12), 5241–5250.
Lee, H. J., Wark, A. W., & Corn, R. M. (2007). Ultrasensitive microarray detection of DNA using enzymatically amplified SPR imaging. In X.-H. N. Xu (Ed.), *New frontiers in ultrasensitive bioanalysis* (pp. 169–194). Hoboken, New Jersey: Wiley-Interscience: John Wiley & Sons, Inc.
Lee, H. J., Wark, A. W., Goodrich, T. T., Fang, S., & Corn, R. M. (2005). Surface enzyme kinetics for biopolymer microarrays: A combination of Langmuir and Michaelis−Menten concepts. *Langmuir, 21*(9), 4050–4057.
McAdam, B., Brennan Fournet, M., McDonald, P., & Mojicevic, M. (2020). Production of polyhydroxybutyrate (PHB) and factors impacting its chemical and mechanical characteristics. *Polymers, 12*.
Mohan, T., Spirk, S., Kargl, R., Doliška, A., Ehmann, H. M. A., Köstler, S., … Stana-Kleinschek, K. (2012). Watching cellulose grow – Kinetic investigations on cellulose thin film formation at the gas–solid interface using a quartz crystal microbalance with dissipation (QCM-D). *Colloids and Surfaces A: Physicochemical and Engineering Aspects, 400*, 67–72.
Nishida, H., & Tokiwa, Y. (1993). Distribution of poly(β-hydroxybutyrate) and poly (ε-caprolactone)aerobic degrading microorganisms in different environments. *Journal of Environmental Polymer Degradation, 1*(3), 227–233.
Palasingh, C., Ström, A., Amer, H., & Nypelö, T. (2021). Oxidized xylan additive for nanocellulose films – A swelling modifier. *International Journal of Biological Macromolecules, 180*, 753–759.
Ravn, J. L., Ristinmaa Amanda, S., Coleman, T., Larsbrink, J., & Geijer, C. (2023). Yeasts have evolved divergent enzyme strategies to deconstruct and metabolize xylan. *Microbiology Spectrum, 11*(3), Article e00245-00223.
Robeson, J. L., & Tilton, R. D. (1996). Spontaneous reconfiguration of adsorbed lysozyme layers observed by total internal reflection fluorescence with a pH-sensitive fluorophore. *Langmuir, 12*, 6104–6113.
Rohm, S., Hirn, U., Ganser, C., Teichert, C., & Schennach, R. (2014). Thin cellulose films as a model system for paper fibre bonds. *Cellulose, 21*(1), 237–249.
Roohi, Zaheer, M. R., & Kuddus, M. (2018). PHB (poly-β-hydroxybutyrate) and its enzymatic degradation. *Polymers for Advanced Technologies, 29*(1), 30–40.
Schaubeder, J. B., Ravn, J. L., Orzan, E. J. Q., Manfrão-Netto, J. H. C., Geijer, C., Nypelö, T., & Spirk, S. (2022). Xylan-cellulose thin film platform for assessing xylanase activity. *Carbohydrate Polymers, 294*, Article 119737.
Song, L., Siguier, B., Dumon, C., Bozonnet, S., & O'Donohue, M. J. (2012). Engineering better biomass-degrading ability into a GH11 xylanase using a directed evolution strategy. *Biotechnology for Biofuels, 5*(1), 3.
Spyros, A., Kimmich, R., Briese, B. H., & Jendrossek, D. (1997). H NMR imaging study of enzymatic degradation in poly(3-hydroxybutyrate) and poly(3-hydroxybutyrate-co-3-hydroxyvalerate). Evidence for preferential degradation of the amorphous phase by PHB depolymerase B from pseudomonas lemoignei. *Macromolecules, 30*(26), 8218–8225.
Squire, P. G., & Himmel, M. E. (1979). Hydrodynamics and protein hydration. *Archives of Biochemistry and Biophysics, 196*(1), 165–177.
The pandas development team. (2023). *pandas-dev/pandas: Pandas (v2.1.1)*. Zendodo.
Tomasi, G., Scandola, M., Briese, B. H., & Jendrossek, D. (1996). Enzymatic degradation of bacterial poly(3-hydroxybutyrate) by a depolymerase from Pseudomonas lemoignei. *Macromolecules, 29*(2), 507–513.
Van Rossum, G., & Drake, F. L. (2009). *Python 3 Reference Manual*. Scotts Valley, CA: CreateSpace, 2009.
Virtanen, P., Gommers, R., Oliphant, T. E., et al. (2020). SciPy 1.0: Fundamental Algorithms for Scientific computing in python. *Nature Methods, 17*(3), 261–272.
Zhang, S., Zhao, S., Shang, W., Yan, Z., Wu, X., Li, Y., Chen, G., Liu, X., & Wang, L. (2021). Synergistic mechanism of GH11 xylanases with different action modes from Aspergillus niger An76. *Biotechnology for Biofuels, 14*(1), 118.